Journal of Nano- and Electronic Physics
Vol. **15** No 6, 06014(7pp) (2023)

Журнал нано- та електронної фізики
Том **15** № 6, 06014(7cc) (2023)

Band Gap Engineering of New Lutetium-based Orthovanadates

V.M. Hreb, Yu.V. Klysko*, M.V. Shpotyuk, L.O. Vasylechko

Lviv Polytechnic National University, 12, Stepan Bandera st., 79013 Lviv, Ukraine

(Received 25 September 2023; revised manuscript received 15 December 2023; published online 27 December 2023)

A series of mixed orthovanadates with nominal composition $Lu_{0.5}R_{0.5}VO_4$ (R = Ce, Pr, Nd, Sm, Eu, Gd, Tb, Dy, Ho, Er, Tm, Yb) were synthesized by a solid-state reaction method in the three-stage annealing process. The single-phase powders with smaller Eu, Tb, Dy, Ho, Er, Tm, Yb were obtained after the second calcined stage at 1200 °C for 5h, while for large Ce, Pr, Nd, Sm needed a third calcining. Rietveld refinement analysis of the crystal structure confirms a zircon-type structure (space group $I4_1/amd$). Furthermore, a linear dependence of the obtained lattice parameters on the ionic radius of the substituted lanthanide R was observed in the mixed $Lu_{0.5}R_{0.5}VO_4$ series. The lattice parameters optimized by ab initio methods are slightly smaller than parameters obtained by Rietveld refinement, which can be explained by inaccuracies in the description of f-electrons using density functional theory (DFT). The transmission and diffuse reflectance spectra of mixed compounds $Lu_{0.5}R_{0.5}VO_4$ are similar to such spectra obtained for corresponding orthovanadates RVO_4. Both obtained spectra indicated significant differences in transmission/reflection intensities between samples annealed at 1200 °C and 1400 °C, but the band gap width remained unchanged, suggesting an improvement their crystallinity. Both experimental and theoretical results reveal a barely noticeable reduction in the band gap observed with a reduction of the ionic radius of the lanthanides. A thorough analysis of the electronic structure of the materials and diffuse reflectance spectra suggests that the position of the *f*-levels of lanthanides is the determining factor in the formation of valence and conduction bands.

Keywords: Rare-earth orthovanadate, Structure characterization, *ab initio* calculation, Band gap, Diffuse reflectance spectra.

DOI: 10.21272/jnep.15(6).06014

PACS numbers: 61.66.Fn, 71.20. – b, 71.27.a, 78.40. –

1. INTRODUCTION

Rare-earth orthovanadates (RVO_4) are widely investigated materials for optical, dielectric and catalytic purposes. It is known, that $LaVO_4$ is characterized by monoclinic symmetry (monazite-type), whereas the other ones (Ce-Lu, Y, Sc) have zircon-type tetragonal structure. $CeVO_4$, $PrVO_4$ and $NdVO_4$ can exist in both polymorphs depending on sample preparation conditions [1-3]. Structural phase transitions as a function of applied pressure are precisely analyzed in the review [3] and correlation between structural phase transitions and functional properties was confirmed. The zircon → scheelite → fergusonite structural phase transition occurs in orthovanadates (RVO_4) with an ionic radius equal to or smaller than samarium, however other rare-earth vanadates, beginning from Nd, show only structural transition from zircon to monazite structure type [3].

Different kinds of synthesis technologies are used for obtaining single-phase rare-earth orthovanadates with expected crystal structure, particle size and application properties. There are solid-state reactions [1, 4, 5], sol-gel [6], sonochemical synthesis [7], hydrothermal and microwave methods [8], and Czochralski process [9]. The verification of various preparation methods of well-known YVO_4 has shown that the sol-gel method allows for reducing the synthesis temperature and particle size, which are an order of magnitude smaller and have higher homogeneity than the samples prepared by solid state reaction [6]. It is known that particle morphology is strongly dependent on the annealing temperatures. The relative density and particle size of $NdVO_4$ and $SmVO_4$, obtained by the solid-state method, increase with increasing heat treatment temperature [5]. The calcined temperature directly influences on functional properties such as efficiency coefficient, resonant frequency, and dielectric constant [4, 5].

Orthovanadates with a tetragonal structure are widely used matrix materials for doping with activator ions, such as rare-earth elements and bismuth, which significantly improve the optical properties of the host matrix and expand the range of their applications. For example, mixed vanadates with a nominal composition of $Lu_{0.74}Y_{0.23}La_{0.01}VO_4$ activated by Yb^{3+} shows attractive optical characteristics and are potential material for application in oscillators and lasers with a wavelength of 1 μm [9]. Bismuth and rare-earth elements (Dy, Er, Ho, Eu, Sm, and Yb) doped yttrium orthovanadates are perspective materials for solar energy due to the efficient conversion of ultraviolet radiation in solar cells [10]. The partial substitution of rare-earth elements allows for a shift of the excitation edge in tetragonal RVO_4 doped with Bi^{3+} [10]. This assumption is confirmed by previous structural and optical studies of the $ScVO_4$-YVO_4 system [11]. The value of V-O bond lengths in zircon-type vanadates correlates well with the bandgap width, and an increase in V-O distances leads to an increase in the bandgap energy [11].

Analysis of obtained results of RVO_4 (R = Y, La, Gd, Lu) [12] host matrixes doped by pair activators Yb^{3+}/Ho^{3+}, Yb^{3+}/Er^{3+}, and Yb^{3+}/Tm^{3+} showed that the most efficient energy transfer occurs via overlap between levels of Yb^{3+} and the Ho^{3+}, Er^{3+}, or Tm^{3+} ions in

* yurii.v.klysko@lpnu.ua

the monoclinic $LaVO_4$ matrix, when excited in the near-infrared spectrum region, which is transparent for living tissues and bones. Such unique optical properties of rare-earth orthovanadates make them promising for industrial, biological, or medical applications as bioprobes or tracking agents [12].

The study of the catalytic properties in terms of hydrogen evolution of nanosized RVO_4 (R = La, Ce, Nd, Sm, Eu, and Gd) [7] orthovanadates showed that $GdVO_4$ acts as a good electrocatalytic material, whereas $CeVO_4$ is the best photocatalyst for the degradation of methylene blue dye. The study of the catalytic properties of the mixed compounds in the $Bi_{1-x}Pr_xVO_4$ system revealed that the praseodymium content significantly affects the structure and morphology, bandgap width, and effective surface area [13]. As a result, samples of pure and 4 % praseodymium-doped bismuth vanadate with monoclinic symmetry, exhibited the best catalytic properties for the degradation of safranin T.

The change in compound content, preparation methods and heat treatment regimes in the $R_{1-x}R_xVO_4$ compounds determine functional properties. Taking into account the above-mentioned results, this work is devoted to establishing the influence of rare-earth elements partial substitution on structural and optical properties of the solid compounds with nominal composition $Lu_{0.5}R_{0.5}VO_4$ (R = Ce, Pr, Nd, Sm, Eu, Gd, Tb, Dy, Ho, Er, Tm, Yb).

2. METHODS

2.1 Synthesis

Mixed orthovanadates $Lu_{0.5}R_{0.5}VO_4$ (R = Ce, Pr, Nd, Sm, Eu, Gd, Tb, Dy, Ho, Er, Tm, Yb) have been prepared by a solid-state reaction method in the frames of ICDD Grant-in-Aid program. Appropriate quantities of rare-earth oxides (CeO_2, Pr_6O_{11}, Nd_2O_3, Sm_2O_3, Eu_2O_3, Gd_2O_3, Tb_4O_7, Dy_2O_3, Ho_2O_3, Er_2O_3, Tm_2O_3, Yb_2O_3, Lu_2O_3, 99.9 % Alfa Aesar) and ammonium metavanadate NH_4VO_3 (99 % Sfera Sim, Lviv, Ukraine) have been ground in an agate mortar and three-time passed through 60um polyamide mesh. The heat treatment procedure of the $Lu_{0.5}R_{0.5}VO_4$ (R = Pr, Nd, Eu, Tb, Dy, Ho, Er, Tm, Yb) powders was performed in three stages in air at 900 °C, 1200 °C and 1400 °C for 24 h, 5 h and 2 h respectively. While other $Lu_{0.5}R_{0.5}VO_4$ (R = Ce, Sm) sequentially annealed in air at 900 °C two times for 5 h and at 1000 °C, 1200 °C, 1300 °C and 1400 °C for 5 h, with intermediate regrinding of the product. The synthesis of the single-phase $Lu_{0.5}Gd_{0.5}VO_4$ is the easiest because it includes only two-stage annealing at 900 °C for 5 h each.

2.2 X-ray Diffraction and Optical Transmission Measurements

X-ray diffraction powder patterns were collected on Aeris Research diffractometer (Malvern PANalytical, the Netherlands) with Cu Kα-radiation (λ = 1.541854 Å) equipped with PIXcel 1D detector.

Transmission spectra have been obtained using FS5 Spectrofluorometer (Edinburgh Instruments, Great British. Diffuse reflection spectra have been measured using Cary 5000 UV-Vis-NIR Spectrophotometer with the installed DRA 2500 UV-Vis-NIR External Diffuse Reflectance Attachment.

2.3 Calculations Procedure

We used ABINIT code [14] to perform first-principle calculations. Geometry optimization has been performed within Broyden-Fletcher-Goldfarb-Shanno minimization using initial lattice parameters and atomic positions, which were derived from measured X-ray diffraction powder patterns of the mixed orthovanadates by the Rietveld method. At this stage, we used GGA-PBE exchange-correlation potential [15] for the self-consistent procedure. The tolerance for stress tensor and interatomic forces were 0.01 GPa and 0.001 eV/A, respectively.

Ground-state properties have been evaluated within PBE0 hybrid functional, based on the projector augmented waves (PAW) [16]. That means, the mixing of the exact Hartree-Fock exchange with the exchange-correlation functional GGA-PBE is performed for d/f - states of a lanthanoid and only inside the atom-centered augmentation sphere. The ratio of the exact exchange (parameter alpha) equals 1/3. The following parameters for the calculations were chosen: the integration in the momentum space was done with 102 k-points in the irreducible part of the Brillouin zone. The number of plane waves needed for the wave function expansion was defined by a cut-off energy of 40 Ha. The cut-off energy for a dielectric matrix was equal to 5.0 Ha.

3. RESULTS AND DISCUSSION

The X-ray phase analysis of the synthesized samples reveals a single-phase tetragonal structure in $Lu_{0.5}R_{0.5}VO_4$ (R = Eu, Gd, Tb, Dy, Ho, Er, Tm, Yb) powders, annealed at 900 °C. All experimental diffraction peaks agree well with references PDF-2 cards No 17-880 ($LuVO_4$), No 15-809 ($EuVO_4$), No 17-340 ($TbVO_4$), No 16-870 ($DyVO_4$), No 15-764 ($HoVO_4$), No 17-199 ($ErVO_4$), No 18-1379 ($TmVO_4$) and No 17-338 ($YbVO_4$), etc. $Lu_{0.5}R_{0.5}VO_4$ (R = Ce, Pr, Nd, Sm) were multiphase. The observed difficulty in phase formations is due to the large difference in the ionic radii of lutetium and corresponding rare-earth elements. The following heat treatment at higher temperatures promoted the formation of a single-phase zircon-type structure (Fig. 1).

The crystal structure refinement of the mixed Lu-based vanadates was performed by Rietveld method in tetragonal space group $I4_1/amd$. Despite the broad diffraction peaks caused by micro deformation or nanosized particles of $Lu_{0.5}Pr_{0.5}VO_4$ powder, a good agreement between the experimental and calculated diffraction patterns was obtained (Fig. 2). The crystal structure of the rest solid solutions is considerably better, and their experimental diffraction patterns have a much higher quality. The last heat treatment procedure noticeably improved the crystallinity of $Lu_{0.5}Nd_{0.5}VO_4$, $Lu_{0.5}Ho_{0.5}VO_4$ and $Lu_{0.5}Er_{0.5}VO_4$ compounds. As a result, the Bragg and profile residuals are reduced. Refined unit cell parameters, atomic coordinates, displacement parameters, Bragg and profile residuals are collected in Table 1 and Table 2. Fig. 3

shows the linear evolution of the obtained lattice parameters of the $Lu_{0.5}R_{0.5}VO_4$ solid solutions as a function of average ionic radii of rare-earth elements.

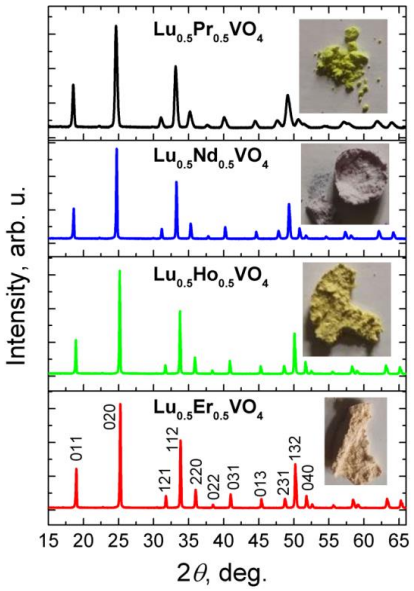

Fig. 1 – Powder diffraction patterns of $Lu_{0.5}R_{0.5}VO_4$ (R = Pr, Nd, Ho, Er) after annealing at 1400 °C. Inserts show color of the samples. Miller indexes of diffraction peaks in tetragonal structure are given in the down panel

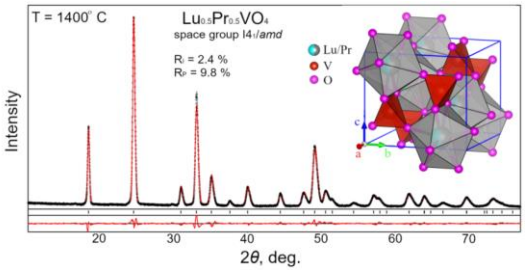

Fig. 2 – Rietveld refinement graphical results of the $Lu_{0.5}Pr_{0.5}VO_4$ powder with zircon-type crystal structure. Insert shows a view of the tetragonal unit cell, which contains two types of polyhedral, where Lu/Pr and V atoms are surrounded by oxygen

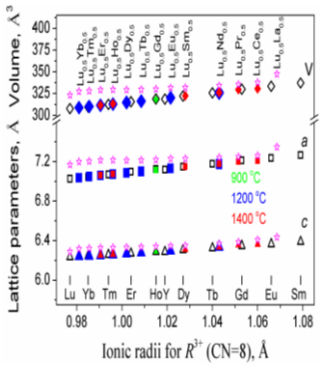

Fig. 3 – Lattice parameters and unit cell volumes of the $Lu_{0.5}R_{0.5}VO_4$ (R = Sm, Tb, Dy, Ho, Tm, Yb, Lu) powders in comparison to "pure" RVO_4 materials. Open and solid symbols represent reference data for RVO_4 compounds and data for investigated Lu-based solid solutions respectively. Magenta stars – lattice parameters optimised by *ab initio* method

Table 1 – Unit cell dimensions, atomic coordinates and displacement parameters, Bragg and profile residuals for $Lu_{0.5}Gd_{0.5}VO_4$ and $Lu_{0.5}R_{0.5}VO_4$ (R = Eu, Tb, Dy, Ho, Er, Tm, Yb) powders after heat treatment of 900 °C and 1200 °C. Space group $I4_1/amd$

Parameters	R in $Lu_{0.5}R_{0.5}VO_4$							
	Eu	Gd	Tb	Dy	Ho	Er	Tm	Yb
a, Å	7.1305(2)	7.1159(2)	7.1009(2)	7.0862(2)	7.0722(4)	7.0596(3)	7.0467(1)	7.0353(6)
c, Å	6.003(2)	6.2886(3)	6.2799(2)	6.2712(2)	6.2618(4)	6.2530(3)	6.2459(1)	6.2409(5)
V, Å^3	320.34(2)	318.43(4)	316.64(3)	314.90(2)	313.18(6)	311.63(5)	310.14(2)	308.89(1)
B_{iso}(Lu/R), Å^2	0.93(2)	1.32(1)	0.80(2)	0.85(2)	1.11(3)	1.12(3)	1.05(2)	0.88(1)
B_{iso}(V), Å^2	0.57(5)	0.45(3)	0.54(5)	0.64(5)	0.51(9)	0.68(8)	0.67(4)	0.57(3)
y/b(O)	0.4288(5)	0.4330(3)	0.4278(5)	0.4297(5)	0.4276(9)	0.4272(9)	0.4276(5)	0.4302(4)
z/c(O)	0.2105(5)	0.2049(3)	0.2106(5)	0.2107(5)	0.2071(9)	0.2100(9)	0.2076(5)	0.2058(4)
B_{iso}(O), Å^2	1.43(11)	2.16(6)	1.30(11)	1.51(11)	1.6(2)	1.9(2)	1.40(9)	1.22(8)
R_I	0.029	0.034	0.032	0.038	0.036	0.032	0.022	0.024
R_P	0.089	0.094	0.095	0.093	0.163	0.1442	0.069	0.061

Table 2 – Unit cell dimensions, atomic coordinates and displacement parameters, Bragg and profile residuals for $Lu_{0.5}R_{0.5}VO_4$ (R = Pr, Nd, Ho, Er) powders after heat treatment of 1400 °C. Space group $I4_1/amd$

Parameters	R in $Lu_{0.5}R_{0.5}VO_4$					
	Ce	Pr	Nd	Sm	Ho	Er
a, Å	7.2075(2)	7.2005(4)	7.1774(1)	7.1467(1)	7.0746(4)	7.0608(6)
c, Å	6.3649(3)	6.3576(3)	6.3371(1)	6.3138(2)	6.2625(3)	6.2538(2)
V, Å^3	330.64(4)	329.62(5)	326.45(2)	322.48(2)	313.43(1)	311.78(1)
B_{iso}(Lu/R), Å^2	1.02(2)	1.20(2)	0.90(2)	1.04(2)	1.12(2)	1.03(1)
B_{iso}(V), Å^2	0.48(5)	1.17(5)	0.57(4)	0.53(5)	0.62(3)	0.67(3)
y/b(O)	0.4167(5)	0.4228(4)	0.4279(4)	0.4200(6)	0.4289(3)	0.4302(3)
z/c(O)	0.2093(5)	0.2068(5)	0.2092(4)	0.2057(6)	0.2044(3)	0.2041(3)
B_{iso}(O), Å^2	1.75(10)	2.51(11)	1.44(9)	1.43(11)	1.23(7)	1.53(6)
R_I	0.041	0.024	0.027	0.038	0.027	0.023
R_P	0.092	0.098	0.071	0.090	0.064	0.055

Structural data of the new Lu-based mixed vanadates as well as their diffractometric characteristics has been included in the last releases (2019, 2021, 2022) of ICDD PDF-2 and PDF-4 database.

Relaxed lattice parameters obtained within geometry optimization by *ab initio* methods are presented in Table 3 and Figure 3 (opened magenta stars). It can be seen that those parameters are bigger than the experimental data (Table 1, Table 2 and Figure 3). This difference is caused by using the GGA-PBE functional, which does not exclude self-interaction, leading to a bigger size of a rare-earth ion. Nevertheless, here we see slightly reducing trends in unit cells in $Lu_{0.5}R_{0.5}VO_4$ with decreasing average ionic radii of rare-earth elements, which point to the observed lanthanide contraction phenomena.

Ab initio calculation of the ground state has shown that $LuVO_4$ and mixed $Lu_{0.5}R_{0.5}VO_4$ compounds are direct band gap materials (Fig. 4). The value of the energy band gap is in the range of 3.54-3.96 eV, while the band gap of $LuVO_4$ is 3.7 eV. Band gap values of the investigated samples $Lu_{0.5}R_{0.5}VO_4$ agree with reference data for RVO_4 (Table 4), which is obtained based on results of different kinds of methods, namely, measurements of the refraction, transmission, absorption and diffuse refraction spectra [7, 17-24].

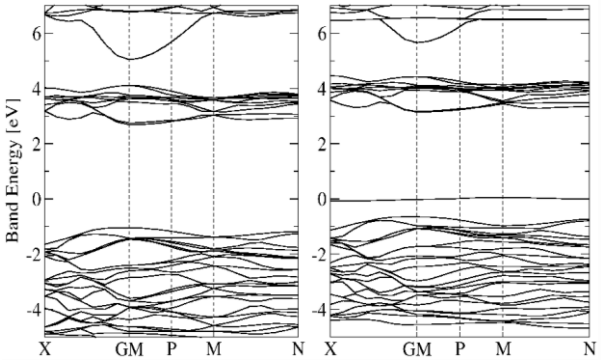

Fig. 4 – Electronic energy band structure in $LuVO_4$ (left panel) and $Lu_{0.5}Nd_{0.5}VO_4$ (right panel). The Fermi level is assumed as the energy reference

The valence band is predominantly composed of *s* states of vanadium and *p* states of vanadium and oxygen (Fig. 5, 6). The values of the band gap E_{gap} for $Lu_{0.5}R_{0.5}VO_4$ compounds formed by the O-V group are collected in Table 5. From the obtained data, it can be seen that the present lanthanide contraction does not affect band gap values. However, the position of the *f*-states in the lanthanides has a decisive influence on E_{gap} (Table 5). The difference between the smallest (R = Tb) and largest (R = Yb) E_{gap} values is close to 10-12 %. This is explained by the fact that *f*-electrons are strongly correlated and localized, meaning that they are practically not hybridized. It is evident that materials $Lu_{0.5}R_{0.5}VO_4$ (R = Sm, Tb, Dy, Yb) in which the Fermi level is located close to the valence band maximum (Figure 6) exhibit significantly higher dielectric permittivity values (Table 5).

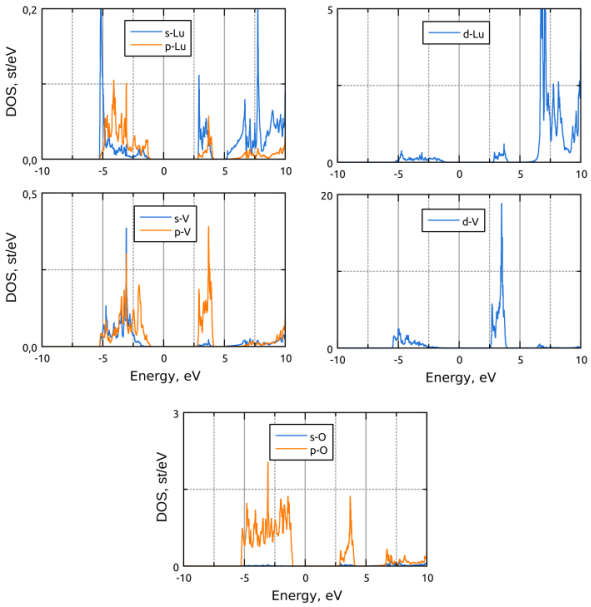

Fig. 5 – Partial Density of States (DOS) in $LuVO_4$. The Fermi level is assumed as the energy reference

Table 3 – Relaxed lattice parameters a and c in $Lu_{0.5}R_{0.5}VO_4$, obtained within *ab initio* geometry optimization

Param	R in $Lu_{0.5}R_{0.5}VO_4$													
	La*	Ce	Pr	Nd	Sm	Eu	Gd	Tb	Dy	Ho	Er	Tm	Yb	Lu
a, Å	7.349	7.261	7.249	7.243	7.230	7.230	7.219	7.215	7.212	7.217	7.214	7.205	7.200	7.17
c, Å	6.438	6.409	6.386	6.369	6.350	6.345	6.340	6.336	6.332	6.331	6.327	6.321	6.316	6.29

* optimisation performed in space group $I4_1/amd$, nevertheless $LaVO_4$ has monoclinic structure.

Table 4 – Experimental values of the band gap energy E_{gap}, obtained for RVO_4 materials

	$LaVO_4$	$CeVO_4$	$PrVO_4$	$NdVO_4$	$EuVO_4$	$GdVO_4$	$DyVO_4$	$HoVO_4$	$ErVO_4$	$LuVO_4$
E_{gap}, eB	3.1^{DRS} [7] 3.5^{refr} [17]	1.8^{refr} [17] 3.2^{abs} [17] 3.36^{trans} [18] 1.8^{DRS} [19]	3.06^{abs} [22]	2.15^{DRS} [7] 3.72^{abs} [17]	3.26^{DRS} [7] 2.07^{DRS} [23]	2.58^{DRS}[7] 3.28^{DRS} [24]	3.65^{DRS} [24]	3.79^{abs} [20]	3.41^{abs} [21]	3.79^{refr} [17] 3.76^{abs} [17]

Reference band gap obtained from spectra analysis of refraction (refr), transmission (trans), absorption (abs) and diffuse refraction spectra (DRS)

Table 5 – Electronic properties of tetragonal crystals $Lu_{0.5}R_{0.5}VO_4$: band gap energy E_{gap} obtained within *ab initio* study as well as experimental ones, defined from diffusion reflectance spectra, and the evaluated dielectric permittivity $\varepsilon_1(0)$

Parameters	R in $Lu_{0.5}R_{0.5}VO_4$						
	La	Ce	Pr	Nd	Sm	Eu	Gd
Ab initio E_{gap}, eV	3.83	3.68	3.75	3.75	3.72	3.76	3.78
Exp. E_{gap}, eV			3.19 (3.21)	3.63 (3.65)		3.59	
Ab initio $\varepsilon_1(0)$	3.81	4.02	3.87	4.44	12.77	3.83	4.36

Parameters	R in $Lu_{0.5}R_{0.5}VO_4$						
	Tb	Dy	Ho	Er	Tm	Yb	Lu
Ab initio E_{gap}, eV	3.54	3.91	3.78	3.79	3.73	3.94	3.76
Exp. E_{gap}, eV	3.00	3.64	3.68 (3.68)	3.68 (3.68)	3.66	3.66	
Ab initio $\varepsilon_1(0)$	8.90	19.57	3.81	4.49	6.18	10.56	3.76

The values in parentheses correspond to the samples annealed at 1400 °C for 2 hours

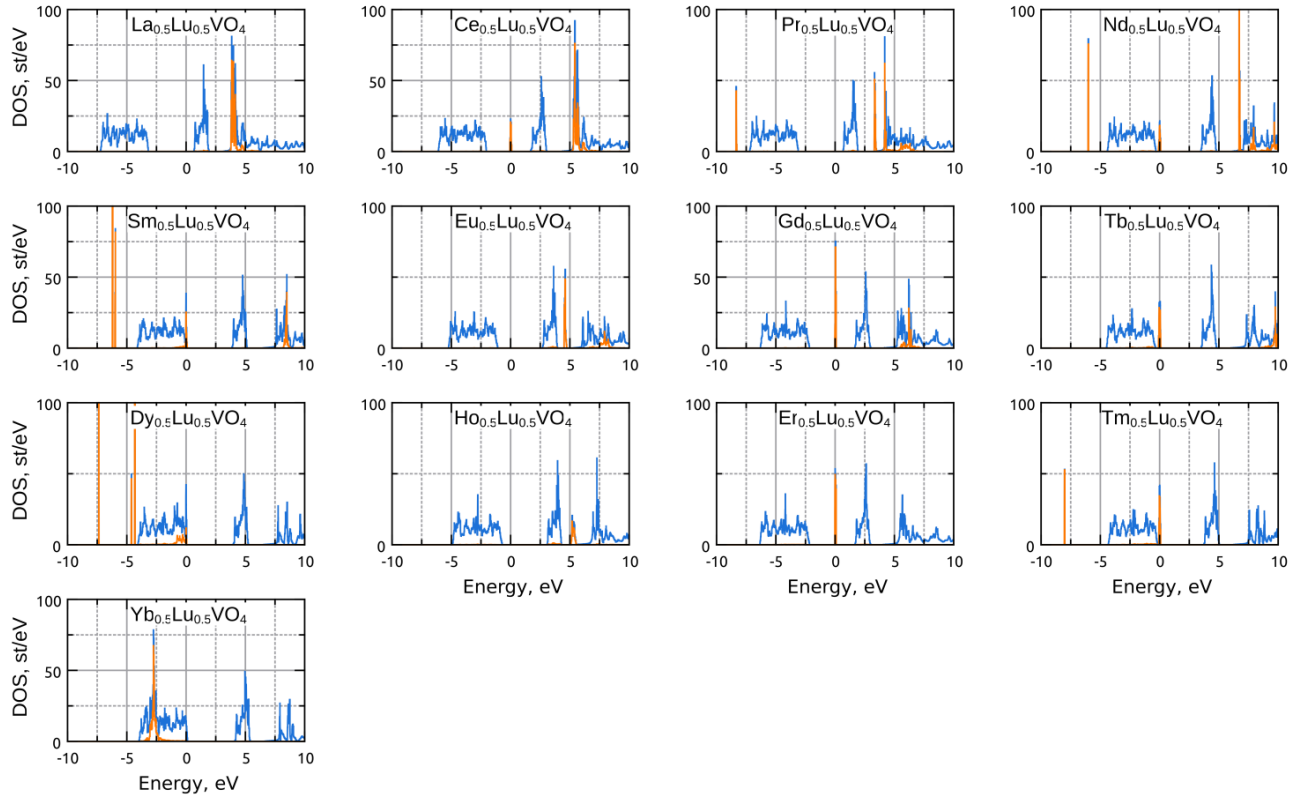

Fig. 6 – Total Density of States (blue curve) and *f*-state contributions of the lanthanide R (orange curve) in $Lu_{0.5}R_{0.5}VO_4$. The Fermi level is assumed as the energy reference

The experimental transmission spectra (Fig. 7) show that the values of E_{gap} are quite lower than those obtained from *ab initio* calculations (Table 5). Intensity growth in the transmission spectrum of samples that underwent additional thermal treatment at a temperature of 1400 °C was revealed. Fig. 7 demonstrates just intensity changes in transmission spectra, but maxima did not shift on the energy scale. It may indicate decreased defects and residual microstresses in the $Lu_{0.5}R_{0.5}VO_4$ materials investigated.

The obtained transmission (Fig. 7) and diffuse reflectance spectra (Fig. 8) of $Lu_{0.5}R_{0.5}VO_4$ solid solution are similar to the "pure"RVO_4 materials. Transitions between electron *f*-levels cause the main absorption bands in both spectra. For example, for Pr^{3+} ions, the absorption peaks at 454 nm (2.73 eV), 478 nm (2.59 eV), 492 nm (2.52 eV), and 602 nm (2.06 eV) are caused by transitions of 4*f* electrons from the $^3H_4$ to $^2P_2$, $^3P_1$, $^3P_0$, and $^3H_6$ levels, respectively (Fig. 8). In the case of Er^{3+} ions, these absorptions at 380, 407, 450, 490, 525, 544, 655, and 798 nm correspond to transitions from the ground state $^4I_{15/2}$ to the excited states $^4G_{11/2}$, $^2H_{9/2}$, $^4F_{5/2}$, $^4F_{7/2}$, $^2H_{11/2}$, $^4S_{3/2}$, $^4F_{9/2}$, and $^4I_{9/2}$, respectively (Fig. 8) [20, 21].

Despite numerous selective studies of the band gap of rare-earth orthovanadates, there is a significant spread of band gap values, which significantly depends on the method of obtaining the material and its microstructure (fig. 9, top panel). the most extensive band gap spread of values for orthovanadates with biggest rare-earth metals are in the range of about 1.8 to 3.8 eV, while the band gap for orthovanadates with small r (approximately from gadolinium to lutetium) ranges from about 3.2 to 4 eV.

The values obtained from *ab initio* calculations and analysis of transmittance and diffuse reflectance spectra for our lutetium-based solid solutions correlate well with reference data. The obtained values of the distances between the vanadium and oxygen atoms, which form the forbidden gap of the rare-earth orthovanadates, are close to each other. From the point of crystal structure [11], the experimental band gap values of lutetium-based orthovanadates must be approximately similar. However, $Lu_{0.5}R_{0.5}VO_4$ solid solutions with terbium and praseodymium (Table 5) are significantly different from others.

4. CONCLUSIONS

Mixed orthovanadates $Lu_{0.5}R_{0.5}VO_4$ (R = Ce, Pr, Nd, Sm, Eu, Gd, Tb, Dy, Ho, Er, Tm, Yb) with zircon-type structure (space group $I4_1/amd$) can be successfully synthesized by solid-state reaction method at annealing temperatures of 900°C, 1200°C and 1400°C.

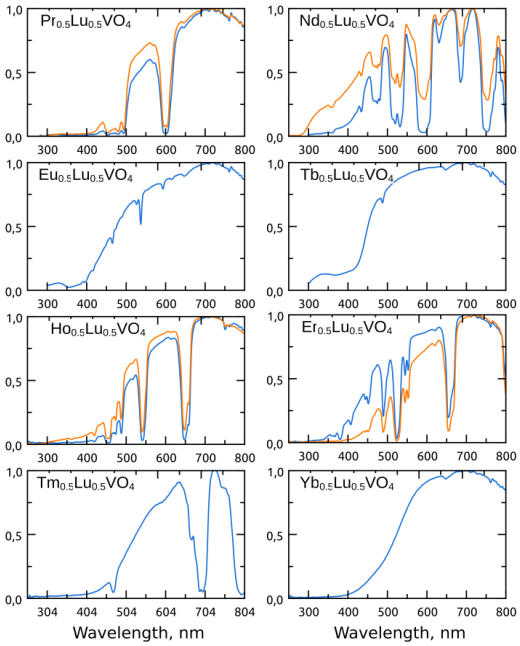

Fig. 7 – The experimental transmittance spectrum of $Lu_{0.5}R_{0.5}VO_4$ crystals: the blue and red line represents samples after a annealing at 1200 °C and 1400 °C, respectively

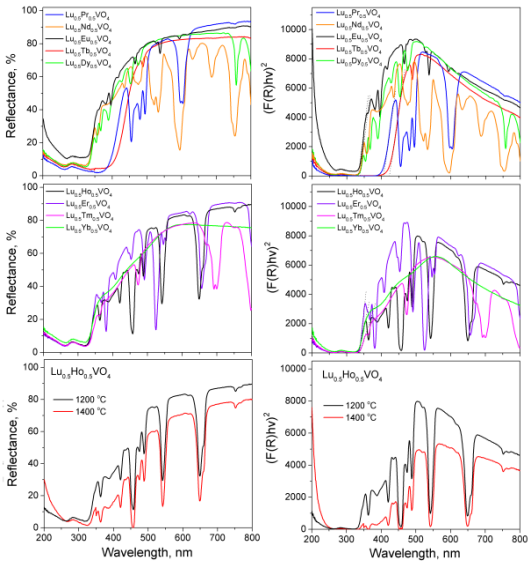

Fig. 8 – The diffuse reflectance spectrum R and the Kubelka-Munk dependence ((F(R) hν)²) for the $Lu_{0.5}R_{0.5}VO_4$ materials. The bottom panel illustrates the effect of annealing temperature on diffuse reflectance spectra of $Lu_{0.5}Ho_{0.5}VO_4$

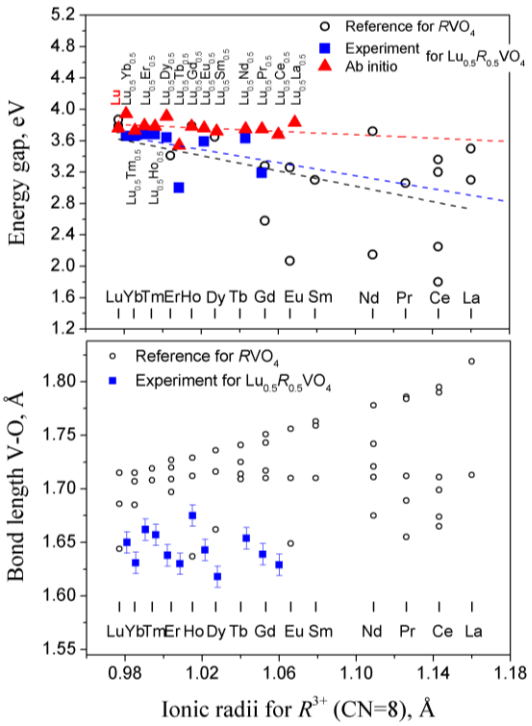

Fig. 9 – Band gap of the reference RVO_4 [7, 17-24] and $Lu_{0.5}R_{0.5}VO_4$ solid solution. The bottom panel shows bond length behavior

Based on the *ab initio* calculation of the electronic and optical properties for $Lu_{0.5}R_{0.5}VO_4$ materials it has been established that the presence of lanthanide compression weakly affects the value of the bandgap. It was confirmed by the results of transmittance and diffuse reflectance spectra measurements. The positioning of the *f*-states of lanthanides is the determining factor in the difficult formation of the band structure and as a result, weak noticeable the difference in the values of the bandgap.

ACKNOWLEDGEMENT

The work was partially supported in parts by ICDD Grant-in-Aid program under Grant N 01-06 and the Ukrainian Ministry of Education and Science (project no. 0121U107736, DB/MODUS).

REFERENCES

1. U. Kolitsch, D. Holtstam, *Eur. J. Mineral.* **16**, 117 (2004).
2. B.C. Chakoumakos, M.M. Abraham. L.A. Boatner, *J. Sol State Chem.* **16**, 197 (1994).
3. D. Errandoneaa, A. B. Garg, *Prog. Mater. Sci.* **97**, 123 (2018).
4. Y. Wang, R. Zuo, C. Zhang, J. Zhang, T. Zhang, *J. Am. Ceram. Soc.* **98**, 1 (2015).
5. W. Li et al., *J. Elec. Mater.* **46**, 1956 (2017).
6. G. Herrera, E. Chavira, J. Jimenez-Mier, L. Banos, J. Guzman, C. Flores, *J. Sol-Gel Sci. Technol.* **46**, 1 (2008).
7. R. Kalai Selvan, A. Gedanken, P. Anilkumar, G. Manikandan, C. Karunakaran, *J. Clust. Sci.* **20**, 291 (2009).
8. S. Mahapatra, S.K. Nayak, G. Madras, T.N. Guru Row, *Ind. Eng. Chem. Res.* **47**, 6509 (2008).
9. B. Zhao et al., *Opt. Mater. Exp.* **8**, 493 (2018).
10. X.Y. Huang et al., *J. Appl. Phys.* **109**, 113526 (2011).
11. L. Vasylechko, A. Tupys, V. Hreb, V. Tsiumra, I. Lutsiuk, Y. Zhydachevskyy, *Inorganics* **6**, 94 (2018).
12. A. Tyminski, T. Grzyb, S. Lis, *J. Am. Ceram. Soc.* **99**, 3300 (2016).
13. V. Sydorchuk, S. Khalameida, N. Shcherban, V. Hreb, V. Mykhaylyk, Y. Zhydachevskyy, L. Vasylechko, *J. Solid State Chem.* **296**, 122002 (2021).

14. X. Gonze, et al., *Comput. Phys. Commun.* **248**, 107042 (2020).
15. J.P. Perdew, K. Burke, M. Ernzerhof, *Phys. Rev. Lett.* **77**, 3865 (1996).
16. P.E. Blöchl, *Phys. Rev. B* **50**, 17953 (1994).
17. V. Panchal, D. Errandonea, A. Segura, P. Rodríguez-Hernandez, A. Muñoz, S. Lopez-Moreno, M. Bettinelli, *J. Appl. Phys.* **110**, 043723 (2011).
18. G. Picardi, F. Varsano, F. Decker, U. Opara-Krasovec, A. Surca, B. Orel, *Electrochimica Acta* **44**, 3157 (1999).
19. M.R. Dolgos, et al., *J. Solid State Chem.* **182**, 1964 (2009).
20. A. Raja, et al., *Electrochimica Acta* **328**, 135062 (2019).
21. S. Obregón, A. Vázquez, D.B. Hernández-Uresti, *J. Mater. Sci.: Mater. Electron.* **29**, 396 (2018).
22. L. Li, Z. Sun, M. Xu, Jiewei Rong, L. Wang, Y. Chen, L. Wang, F. Wang, *Micro Nano Lett.* **15**, 170 (2020).
23. Y. Che, S. Sun, P. Tang, H. Chen, Y. Ding, *Integr. Ferroelectr.* **227**, 231 (2022).
24. J. Jovanović, et al., *Opt. Mater.* **76**, 308 (2018).

Заборонена зона нових ортованадатів на основі лютецію

В.М. Греб, Ю.В. Клишко, М.В. Шпотюк, Л.О. Василечко

Національний університет «Львівська політехніка», вул. Степана Бандери, 12, 79013 Львів, Україна

Ряд змішаних ортованадатів номінального $Lu_{0.5}R_{0.5}VO_4$ (R = Ce, Pr, Nd, Sm, Eu, Gd, Tb, Dy, Ho, Er, Tm, Yb) синтезовано методом твердофазної реакції в тристадійний процес відпалу. Однофазні порошки з меншими Eu, Tb, Dy, Ho, Er, Tm, Yb отримували після другої стадії прожарювання при 1200 °C протягом 5 годин, тоді як для великих Ce, Pr, Nd, Sm потребували третього прожарювання. Уточнений аналіз кристалічної структури Рітвельдом підтверджує структуру типу циркону (просторова група I41/amd). Крім того, у змішаному ряді $Lu_{0.5}R_{0.5}VO_4$ спостерігалася лінійна залежність отриманих параметрів ґратки від іонного радіуса заміщеного лантаноїду R. Параметри решітки, оптимізовані методами ab initio, дещо менші за параметри, отримані за допомогою уточнення Рітвельда, що можна пояснити неточностями в описі f-електронів за допомогою теорії функціоналу густини (DFT). Спектри пропускання та дифузного відбиття змішаних сполук $Lu_{0.5}R_{0.5}VO_4$ подібні до спектрів, отриманих для відповідних ортованадатів RVO_4. Обидва отримані спектри вказують на значні відмінності в інтенсивності пропускання/відбиття між зразками, відпаленими при 1200 і 1400 °C, але ширина забороненої зони залишається незмінною, що свідчить про покращення їх кристалічності. Як експериментальні, так і теоретичні результати показують ледь помітне зменшення забороненої зони, що спостерігається при зменшенні іонного радіуса лантаноїдів. Ретельний аналіз електронної структури матеріалів і спектрів дифузного відбиття свідчить про те, що положення *f*-рівнів лантаноїдів є визначальним фактором у формуванні валентних зон і зон провідності.

Ключові слова: Рідкоземельний ортованадат, Характеристика структури, Розрахунок ab initio, Заборонена зона, Спектр дифузного відбиття.